The Supplement of Tropical cyclone amplifies anthropogenic influences on aerosol-cloud interactions over the South China Sea

Hengjia Ou[1,2], Mingfu Cai[3], Haichao Wang[1], Xue Ni[4], Shixin Mai[1], Qibin Sun[5], Baoling Liang[6], Kunpeng Chen[7], Tao Deng[2], Sun Jiaren[3], Shengzhen Zhou[1], and Jun Zhao[1,†]

[1] School of Atmospheric Sciences, Sun Yat-sen University, and Southern Marine Science and Engineering Guangdong Laboratory (Zhuhai), Zhuhai 519082, China
[2] Institute of Tropical and Marine Meteorology, China Meteorological Administration, Guangzhou 510640, China
[3] Guangdong Province Engineering Laboratory for Air Pollution Control, Guangdong Provincial Key Laboratory of Water and Air Pollution Control, South China Institute of Environmental Sciences, MEE, Guangzhou 510655, China
[4] Guangzhou Ecological and Agricultural Meteorological Center, Guangzhou 511430, China
[5] Guangzhou Sub-branch of Guangdong Ecological and Environmental Monitoring Center, Guangzhou 510006, China
[6] Dongguan Meteorological Bureau, Dongguan 523086, China
[7] State Key Laboratory of Regional Environment and Sustainability, School of Environment, Tsinghua University, Beijing 100084, China
[†] Deceased, 10/2024
Correspondence to: Mingfu Cai (mingfu0721@hotmail.com) and Haichao Wang (wanghch27@mail.sysu.edu.cn)

Text S1-S4

Figure S1-S14

Table S1-S2

Text S1 The SMCA setting

Due to a malfunction of the flow sensor in column B during both cruises, only data from column A are used in this study. During SMCA operation, aerosol particles were first dried using a Nafion dryer, neutralized with a bipolar neutralizer, and then size-selected by the DMA. The classified particles were split between the CPC (1 L min^{-1}) for total particle counting and the CCNc (0.5 L min^{-1}) for CCN counting at a controlled supersaturation (SS). To maintain stable flow through the DMA, dilution air (0.5 L min^{-1}) was added to the CPC inlet; its effect on the PNSD was corrected during data processing (Fig. S3).

During the measurement period, the CCNc supersaturations (SS) were set to 0.2%, 0.4%, and 0.7%. Each supersaturation level was maintained for 20 min, during which the DMA completed a full scan every 5 min. Supersaturation transitions between adjacent SS levels (e.g., 0.2%→0.4%, 0.4%→0.7%) typically stabilized within seconds to tens of seconds, while transitions from 0.7% to lower SS (0.1-0.2%) required up to ~5 min. Only scans with stable CCNc temperature and supersaturation throughout the DMA cycle were included in the analysis.

Text S2 Data quality control

To ensure the reliability of atmospheric measurements over the SCS and to minimize contamination from ship emissions, we applied a series of data screening procedures following previous studies.[1-3] First, organic compounds, NO_2, and N_{CN} were used as tracers of ship exhaust, and abrupt spikes in their concentrations were identified as indicators of contamination. Second, the relative positions of the sampling inlet and the ship's exhaust stack were considered. In this study, data were removed when the relative wind direction was between 150° and 220° and the relative wind speed was below 2.5 m s^{-1} (Fig. S11).

After applying these filters, 90.1% of the data (10-minute resolution) were classified as clean and retained for subsequent analysis. The time series before and after quality control was shown in Fig. S12. Besides, the time series of reactive gas was shown in Fig. S13.

Text S3 PMF analysis

The Positive Matrix Factorization (PMF) Evaluation Tool (PET) [4], which is based on a bilinear model, was used to resolve the sources of organic aerosols. The model can be expressed as:

$$X_{ij} = g_{ik} \times f_{kj} + e_{ij} \quad (1)$$

where X_{ij} (with i and j denoting sample and species indices, respectively) represents the organic mass concentrations measured by the ToF-ACSM. The matrix X is decomposed into a factor-contribution matrix G and a factor-profile matrix F, while e_{ij} denotes the residual for each sample–species pair. The number of factors k is determined by the user. The optimal solution is obtained using a least-squares approach that minimizes the objective function Q:

$$Q_m = \left(\frac{e_{ij}}{\varepsilon_{ij}}\right)^2 \quad (2)$$

where ε_{ij} represents the measurement uncertainty. The value of Q is iteratively minimized to achieve the best factorization.

Text S4 Fitting of log-normal modes to particle number size distributions and effective diameter calculation

The multi-lognormal distribution function (Eq. (8)) is used to parameterize and optimize the descriptions of the measured PNSD [5] and is widely applied in aerosol research [2, 6, 7]. An automatic mode-fitting algorithm (Hussein et al., 2005) is used to generate the model-fitted results.

$$f\left(D_p, \overline{D}_{pg,i}, N_i, \sigma_{g,i}\right) = \sum_{i=1}^{n} \frac{N_i}{\sqrt{2\pi}\log(\sigma_{g,i})} \times \exp\left[-\frac{\left[\log D_p - \log \overline{D}_{pg,i}\right]^2}{2\left(\log \sigma_{g,i}\right)^2}\right] \quad (3)$$

where D_P is the diameter of a particle. Each lognormal mode is characterized by three parameters: the mode number concentration (N_i), geometric variance ($\sigma_{g,i}$), and geometric mean diameter (GMD, $\overline{D}_{pg,i}$). The total number of lognormal modes used to describe the PNSD is denoted by n. These modes are fitted using an algorithm applied to each particle size distribution, with one to three log-normal distributions used per time step. The algorithm classifies the PNSD into nucleation, Aitken, and accumulation modes based on their geometric mean diameters (GMDs). The GMD for nucleation modes (GMD1) typically ranges from 3 to 30 nm, for Aitken modes (GMD2) from 30 to 100 nm, and for accumulation modes (GMD3) above 100 nm (Heintzenberg, 1994; Hussein et al., 2005; Zhu and Wang, 2024).

The effective diameter (D_{eff}) could be calculated as following:

$$D_{eff} = \sum_i \frac{D_i \times N_i}{N_{tot}} \quad (4)$$

where D_i is the i-th particle diameter, N_i is the corresponding particle number concentration for the i-th diameter, and N_{tot} is the total particle number concentration.

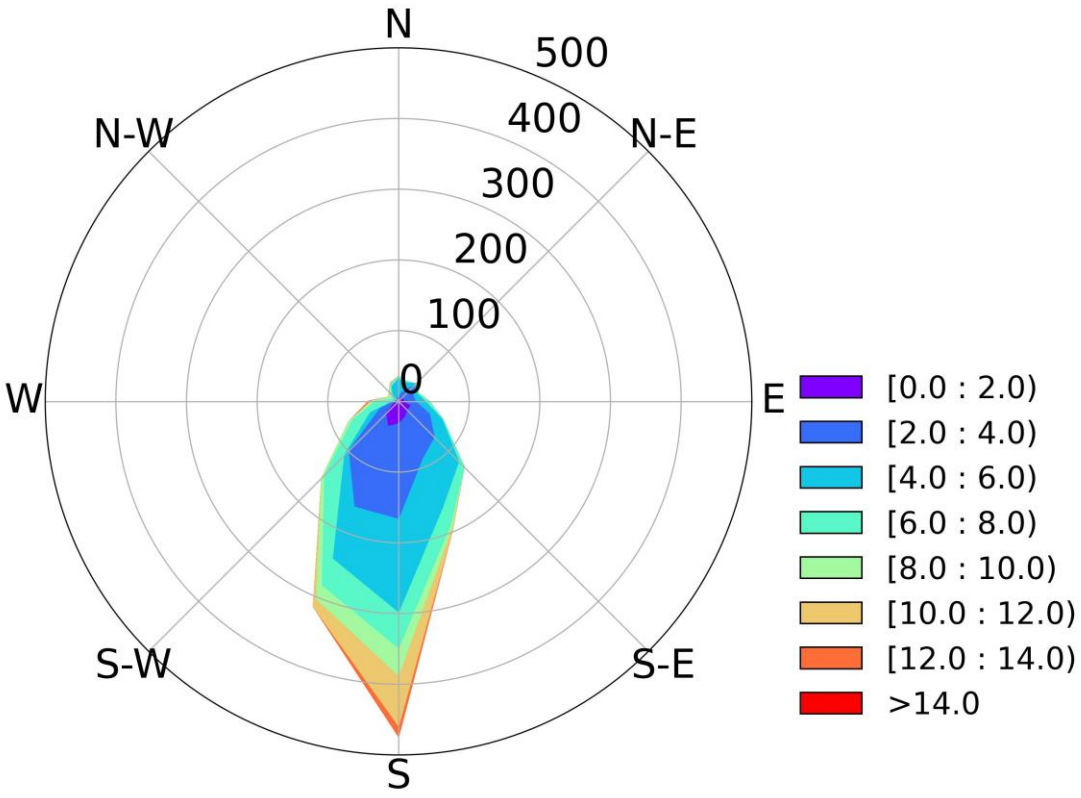

Figure S1. The windrose diagram during the ship measurement period.

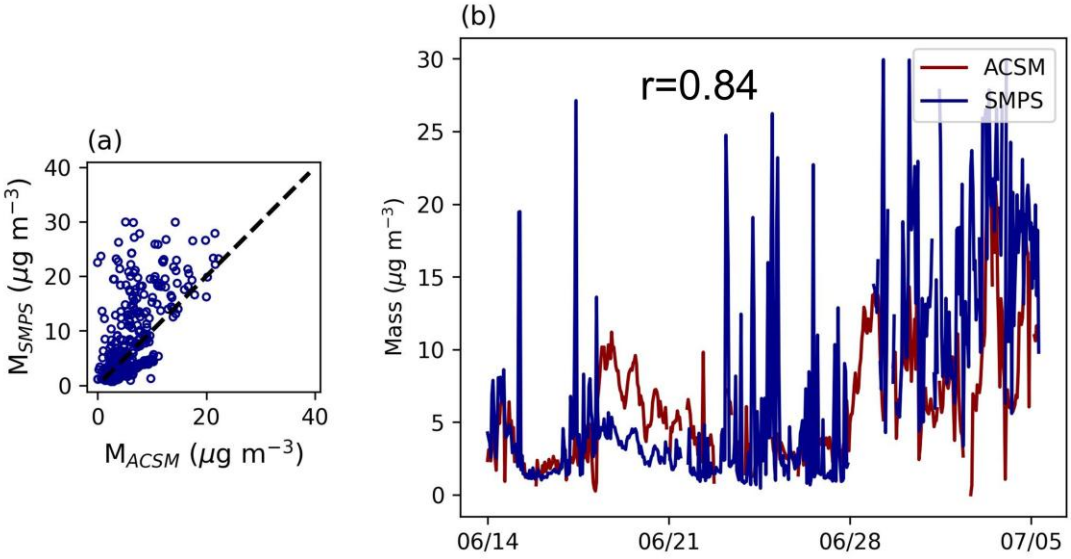

Figure S2. The scatter of mass concentration from ACSM and SMPS (a) and the timeseries of mass concentration from ACSM and SMPS (b).

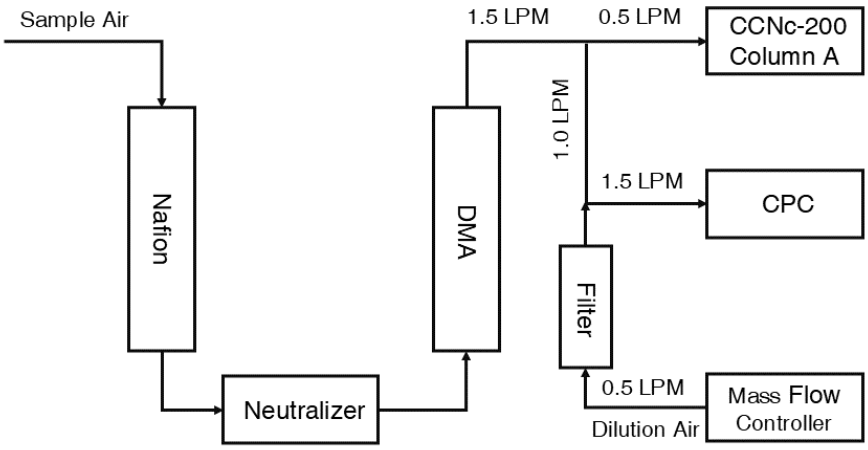

Figure S3. Instrument setup of the SMCA system.

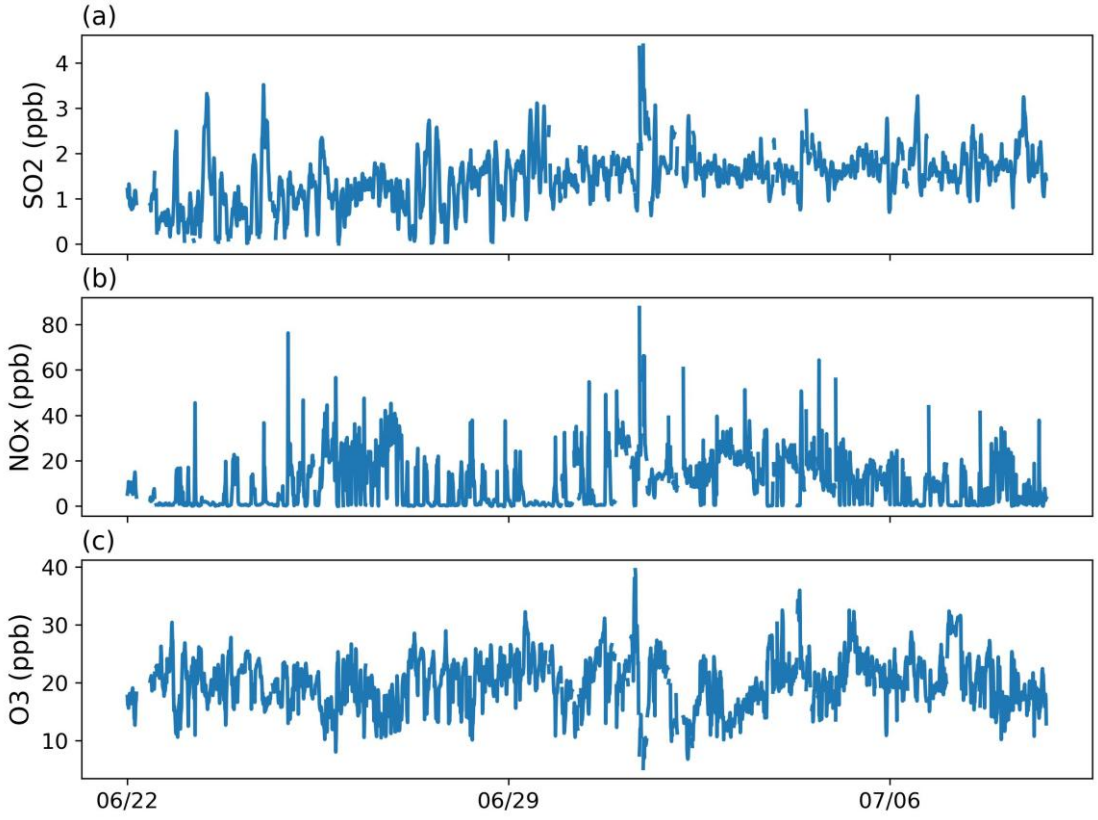

Figure S4. The timeseries of SO_2, NOx, and O_3

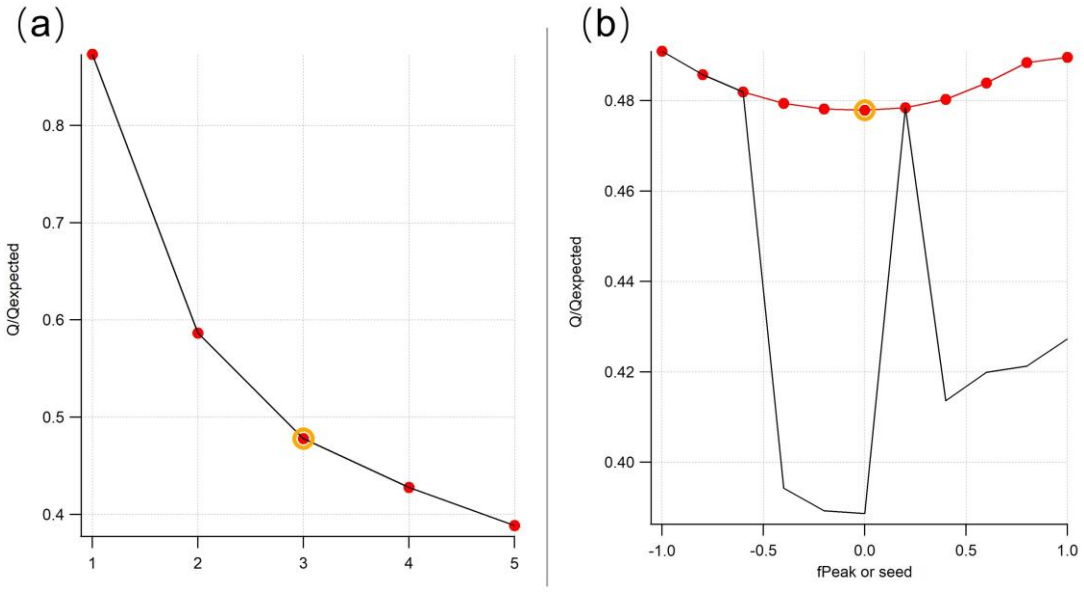

Figure S5. The diagnostic plots of OA PMF: The Q/Qexp in different number of factors (a) and the Q/Qexp in different fpeak (b)

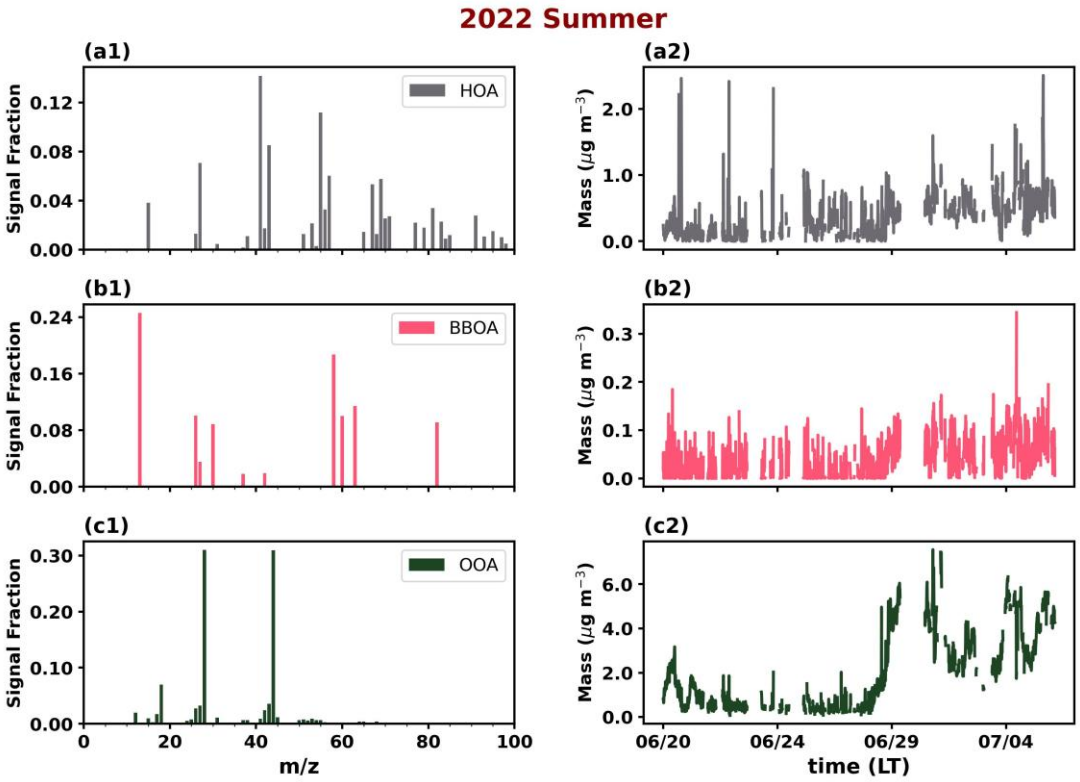

Figure S6. The mass spectrum of HOA (a1), BBOA (b1), and OOA (c1) and the timeseries of HOA (a2), BBOA (b2), and MO-OOA (c2).

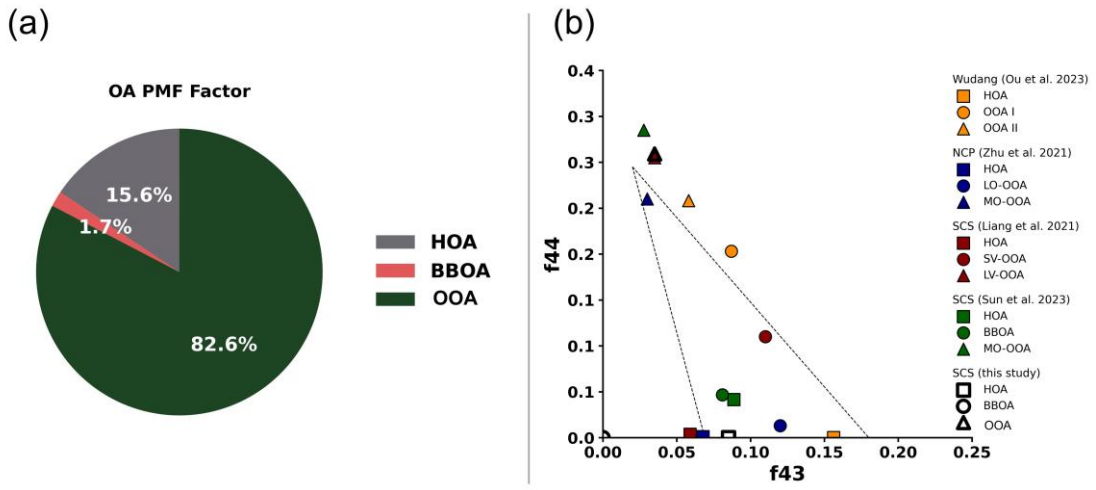

Figure S7. The mass fraction of HOA, BBOA, and OOA and the f44 vs f43 plot between factors in this study and other studies [8-11].

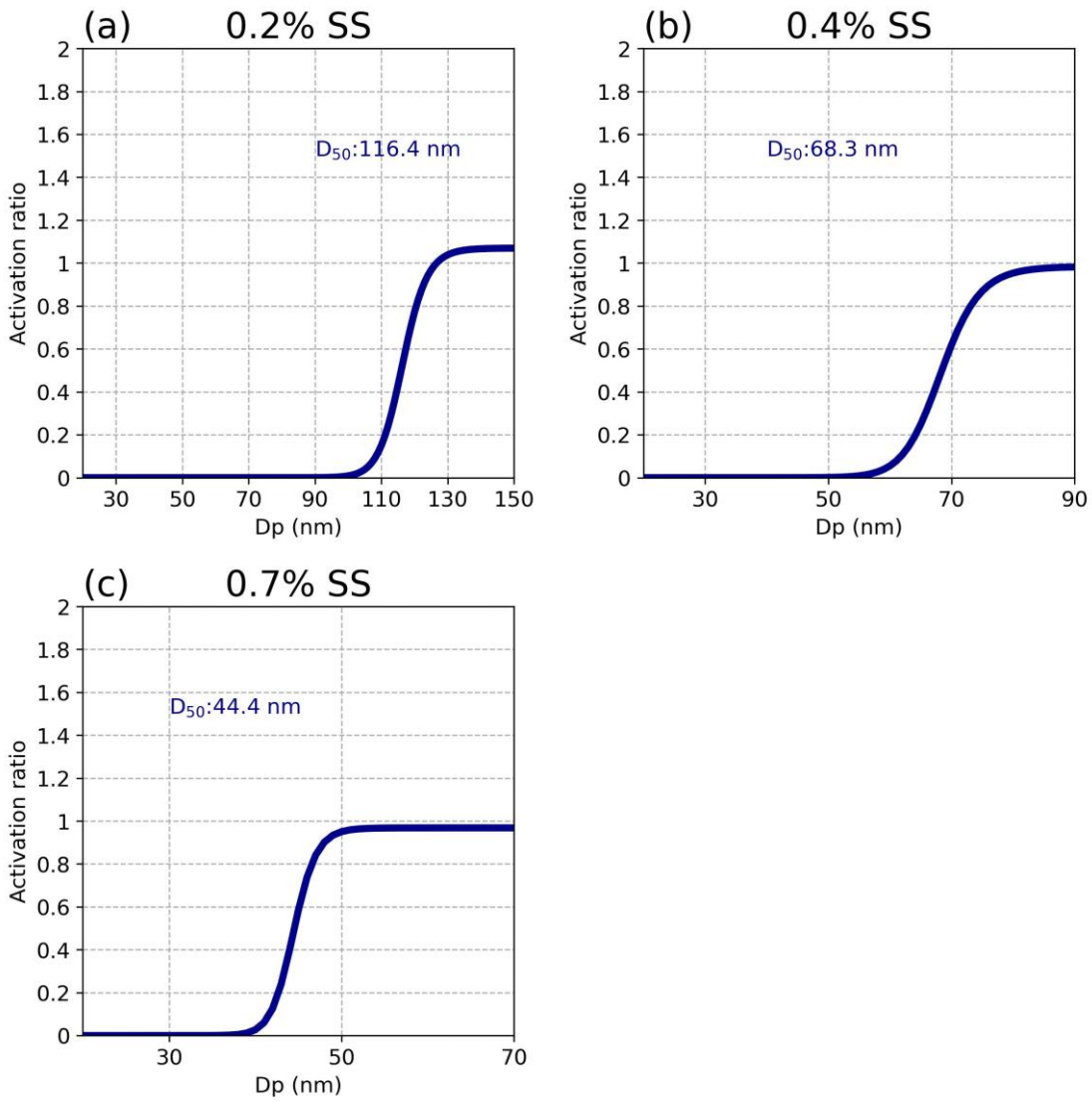

Figure S8. The average fitting result of SMCA method at 0.2% (a), 0.4% (b), and 0.7% (c) SS in this study.

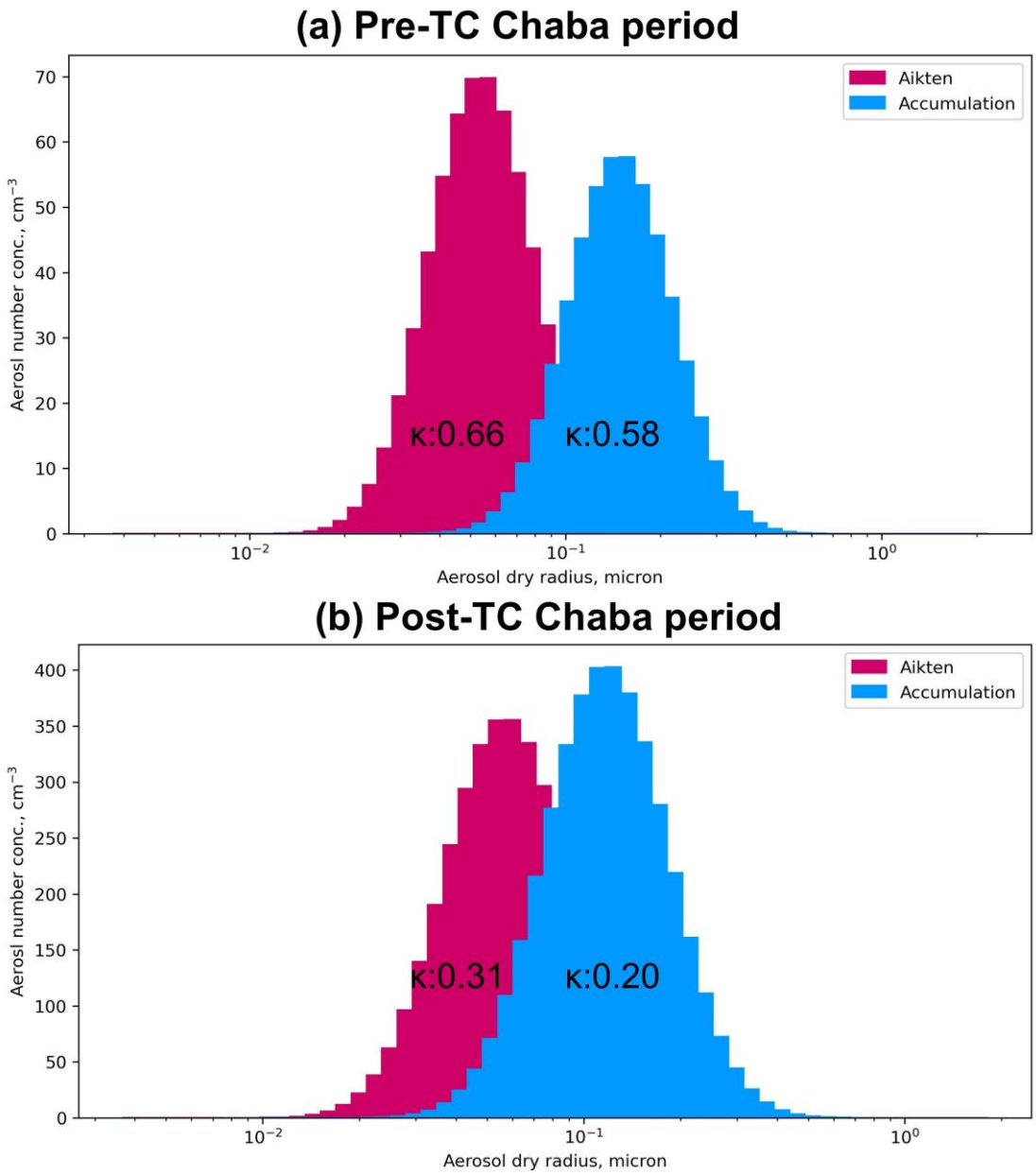

Figure S9. The input of aerosol size distribution and their hygroscopicity (a) during pre-TC Chaba period and (b) post-TC Chaba period in Pyrcel model

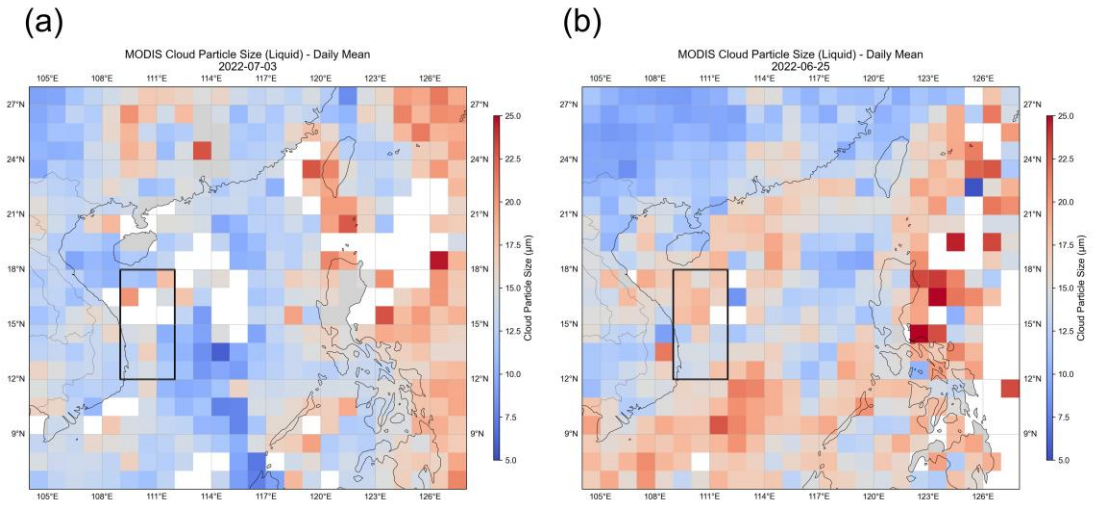

Figure S10. The example of daily liquid cloud particle size from modis data during pre-TC Chaba period(a) and post-TC Chaba period (b).

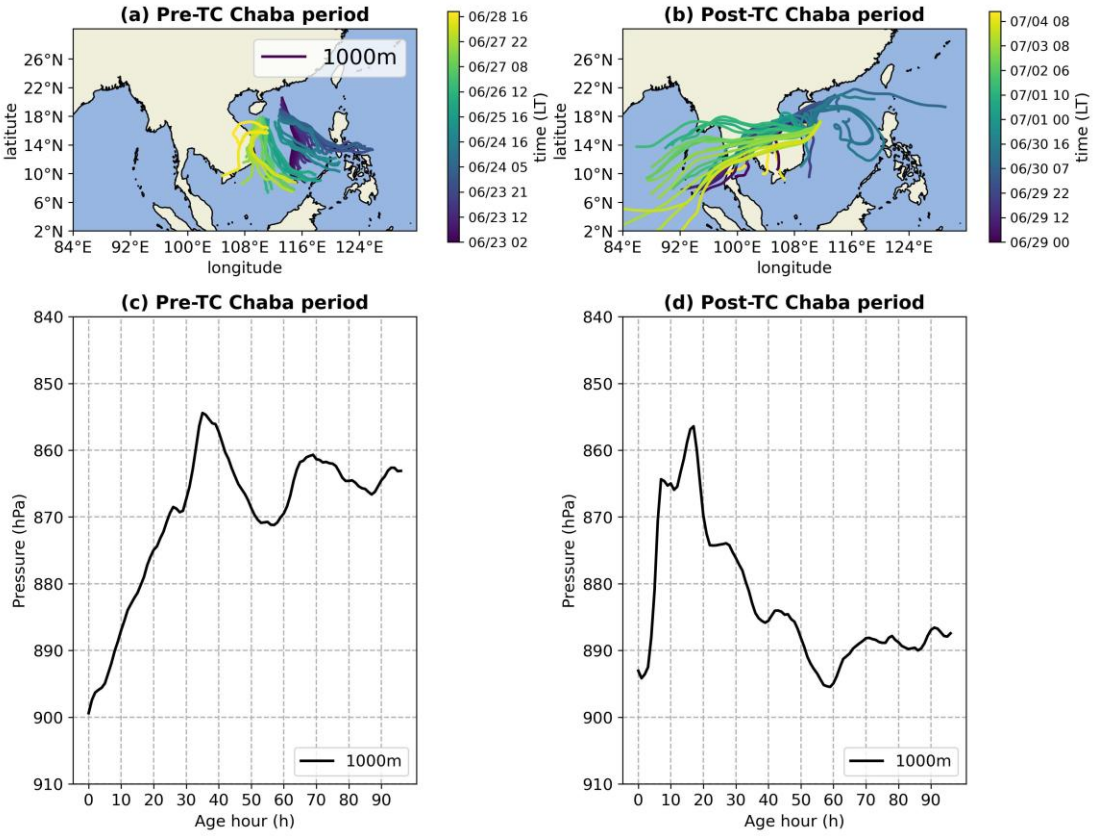

Figure S11. The backward tracjectories (a) and their average altitude in different age hours (c) during pre-TC Chaba period; The backward tracjectories (b) and their average altitude in different age hours (d) during post-TC Chaba period

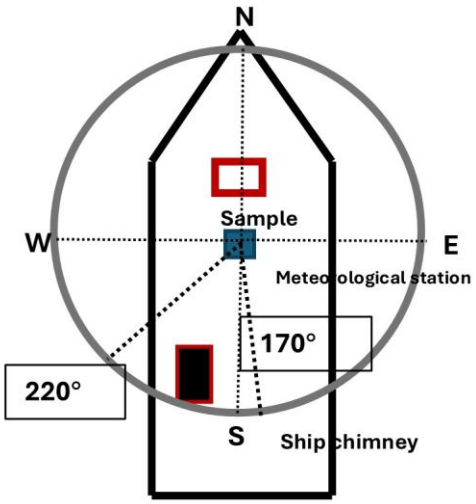

Figure S12. The selected wind direction range in data quality control

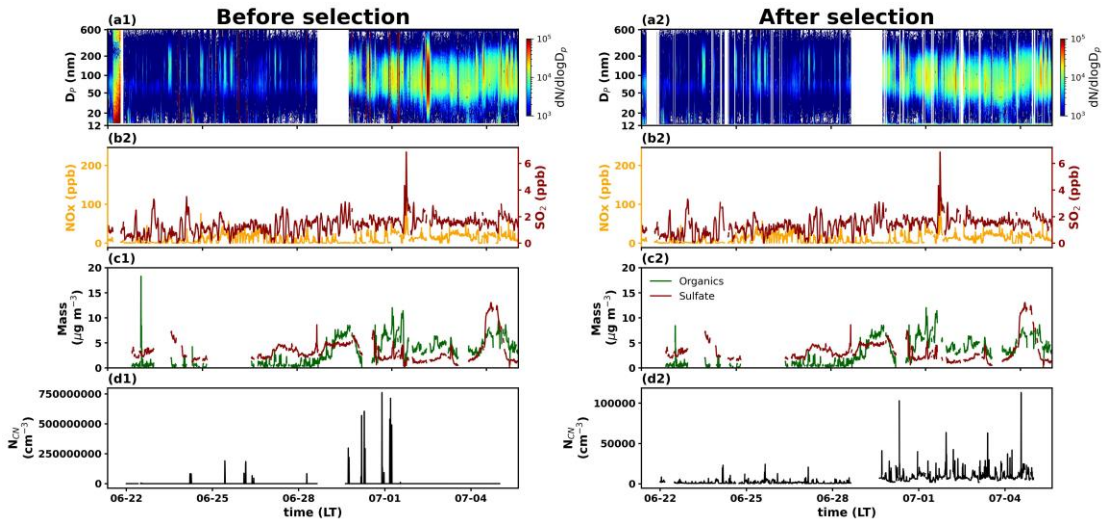

Figure S13. The timeseries of particle number size distribution (PNSD) (a1), gases (NOx and SO2) (b1), organics and sulfate (c1), and total particle number concentration (N_{CN}) (d1) before data quality control; The timeseries of PNSD (a2), gases (NOx and SO2) (b2), organics and sulfate (c2), and N_{CN} (d2) after data quality control

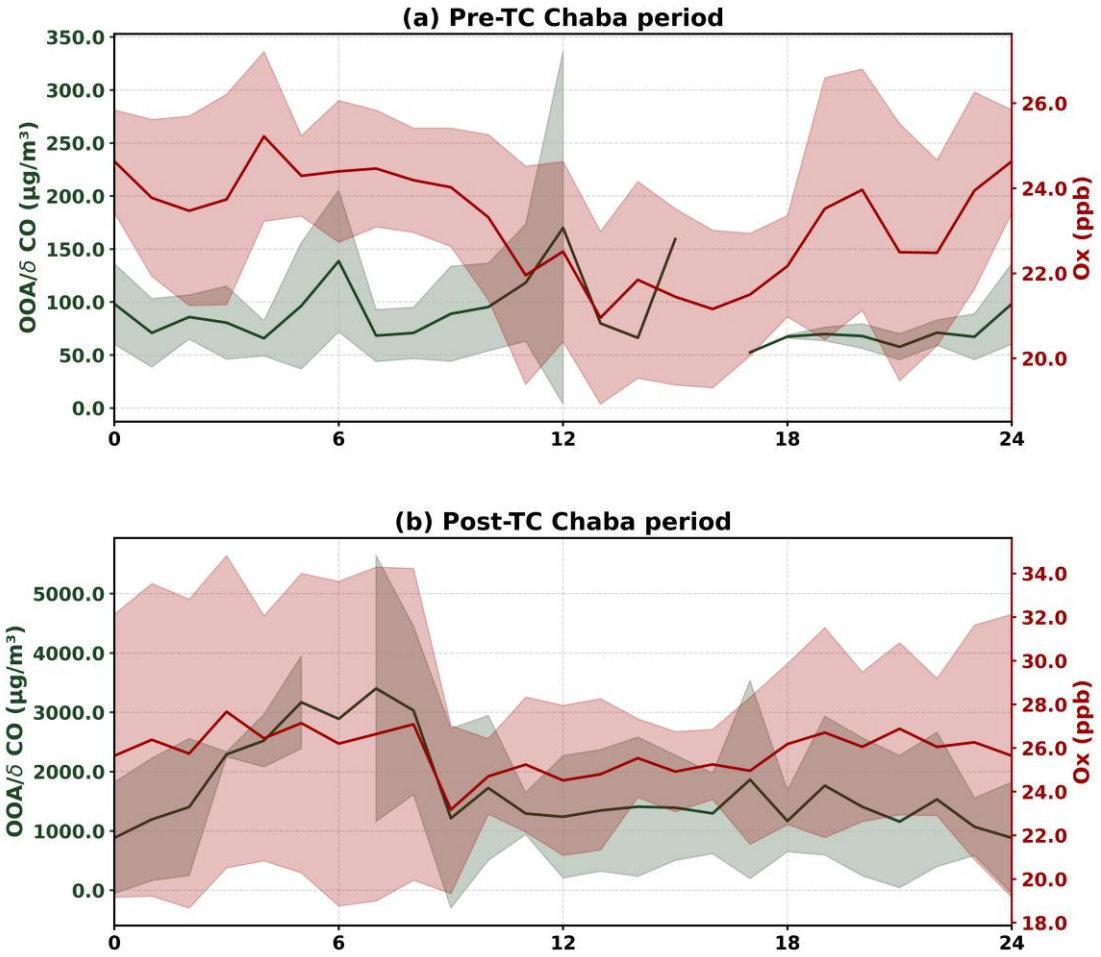

Figure S14. The diurnal pattern of OOA and O_X during pre-TC Chaba period (a) and post-TC Chaba period (b)

Table S1 The input parameters in Pyrcel models during pre-TC Chaba and post-TC Chaba periods

	Pre-TC Chaba	Post-TC Chaba
T (K)	304	304
P (hPa)	1005	998
RH (%)	77	82
D_{Aikten} (nm)	57	60
s_{Aikten}	1.42	1.49
N_{Aikten} (cm^{-3})	626	3607
$D_{\mathrm{Accumulation}}$ (nm)	157	124
$s_{\mathrm{Accumulation}}$	1.46	1.55
$N_{\mathrm{Accumulation}}$ (cm^{-3})	517	4084
κ_{Aikten}	0.66	0.31
$\kappa_{\mathrm{Accumulation}}$	0.58	0.20

Table S2 The fitting result of critical maximum supersaturations and cloud droplet concentration under updraft velocity range from 0.1 to 2 m s^{-1}

Updraft velocity (m s^{-1})	S_{max} (%, Pre-TC Chaba)	S_{max} (%, Post-TC Chaba)	N_C (cm^{-3}, Pre-TC Chaba)	N_C (cm^{-3}, Post-TC Chaba)
0.1	0.03	0.03	326	465
0.3	0.06	0.04	503	1025
0.5	0.08	0.05	668	1804
0.8	0.12	0.07	832	2448
1	0.14	0.08	903	2849
1.3	0.17	0.09	968	3420
1.5	0.18	0.10	1023	3667
1.8	0.21	0.11	1066	4296
2	0.23	0.11	1066	4296

Reference

[1] Huang, S.; Wu, Z.; Poulain, L.; van Pinxteren, M.; Merkel, M.; Assmann, D.; Herrmann, H.; Wiedensohler, A. Source apportionment of the organic aerosol over the Atlantic Ocean from 53° N to 53° S: significant contributions from marine emissions and long-range transport. *Atmos. Chem. Phys.* **2018**, *18* (24), 18043-18062. DOI: 10.5194/acp-18-18043-2018.

[2] Cai, M.; Liang, B.; Sun, Q.; Zhou, S.; Chen, X.; Yuan, B.; Shao, M.; Tan, H.; Zhao, J. Effects of continental emissions on cloud condensation nuclei (CCN) activity in the northern South China Sea during summertime 2018. *Atmos. Chem. Phys.* **2020**, *20* (15), 9153-9167. DOI: 10.5194/acp-20-9153-2020.

[3] Ou, H.; Cai, M.; Zhang, Y.; Ni, X.; Liang, B.; Sun, Q.; Mai, S.; Sun, C.; Zhou, S.; Wang, H.; et al. Measurement report: Cloud condensation nuclei (CCN) activity in the South China Sea from shipborne observations during the summer and winter of 2021 – seasonal variation and anthropogenic influence. *Atmos. Chem. Phys.* **2025**, *25* (4), 2495-2513. DOI: 10.5194/acp-25-2495-2025.

[4] Ulbrich, I. M.; Canagaratna, M. R.; Zhang, Q.; Worsnop, D. R.; Jimenez, J. L. Interpretation of organic components from Positive Matrix Factorization of aerosol mass spectrometric data. *Atmos. Chem. Phys.* **2009**, *9* (9), 2891-2918. DOI: 10.5194/acp-9-2891-2009.

[5] Heintzenberg, J. Properties of the Log-Normal Particle Size Distribution. *Aerosol Sci Tech* **1994**, *21* (1), 46-48. DOI: 10.1080/02786829408959695.

[6] Boyer, M.; Aliaga, D.; Pernov, J. B.; Angot, H.; Quéléver, L. L. J.; Dada, L.; Heutte, B.; Dall'Osto, M.; Beddows, D. C. S.; Brasseur, Z.; et al. A full year of aerosol size distribution data from the central Arctic under an extreme positive Arctic Oscillation: insights from the Multidisciplinary drifting Observatory for the Study of Arctic Climate (MOSAiC) expedition. *Atmos. Chem. Phys.* **2023**, *23* (1), 389-415. DOI: 10.5194/acp-23-389-2023.

[7] Zhu, K.; Wang, L. A comprehensive study on the validation and application of multi-lognormal distribution models for atmospheric particles. *Atmos Environ.* **2024**, *338*, 120813. DOI: 10.1016/j.atmosenv.2024.120813.

[8] Ou, H. J.; Cai, M. F.; Liang, B. L.; Sun, Q. B.; Zhou, S. Z.; Xu, Y. S.; Ren, L. H.; Zhao, J. Characterization, Sources, and Chemical Processes of Submicron Aerosols at a Mountain Site in Central China. *J Geophys Res-Atmos* **2023**, *128* (16), e2022JD038258. DOI: https://doi.org/10.1029/2022JD038258 (acccessed 2024/11/02).

[9] Zhu, Q.; Cao, L.-M.; Tang, M.-X.; Huang, X.-F.; Saikawa, E.; He, L.-Y. Characterization of Organic Aerosol at a Rural Site in the North China Plain Region: Sources, Volatility and Organonitrates. *Adv. Atmos. Sci* **2021**, *38* (7), 1115-1127. DOI: 10.1007/s00376-020-0127-2.

[10] Liang, B.; Cai, M.; Sun, Q.; Zhou, S.; Zhao, J. Source apportionment of marine atmospheric aerosols in northern South China Sea during summertime 2018. *Environ. Pollut.* **2021**, *289*, 117948. DOI: 10.1016/j.envpol.2021.117948.

[11] Sun, Q.; Liang, B.; Cai, M.; Zhang, Y.; Ou, H.; Ni, X.; Sun, X.; Han, B.; Deng, X.; Zhou, S.; et al. Cruise observation of the marine atmosphere and ship emissions in South China Sea: Aerosol composition, sources, and the aging process. *Environ. Pollut.* **2023**, *316* (Pt 1), 120539. DOI: 10.1016/j.envpol.2022.120539.